Heliyon 9 (2023) e13267

Contents lists available at ScienceDirect

Heliyon

journal homepage: www.cell.com/heliyon

Research article

Adsorption mechanism of Cr(VI) on woody-activated carbons

Hua Wang [a,b,*], Wencheng Wang [a], Song Zhou [a], Xuchun Gao [a,b]

[a] College of Chemistry and Chemical Engineering, Yulin City, 719000, China
[b] Shaanxi Provincial Key Laboratory of Clean Utilization of Low-Modified Coal, Yulin City, 719000, China

ARTICLE INFO

Keywords:
Cr(VI) removal
Woody-activated carbon
Isotherm
Adsorption mechanism
Kinetic

ABSTRACT

To provide guidance for the selection of woody-activated carbon in the treatment of wastewater containing hexavalent chromium (Cr(VI)), the adsorption tests on two varieties of commercial woody-activated carbon powder from different manufacturers were carried out. The physico-chemical properties and structural characteristics of activated carbon were studied by using elemental, chemical, and instrumental analyses. The adsorption mechanism of Cr(VI) was discussed by investigating the factors affecting the removal of hexavalent chromium. The two kinds of woody-activated carbon have microporous and mesoporous structures. Commercial woody-activated carbon No.1 (ACI) has a more extensive specific surface area and a better-developed pore structure. While ACI exhibits a higher adsorption capability when the content of Cr(VI) is high, commercial woody-activated carbon No.2 (AC) can remove hexavalent chromium fast when the concentration is low. A rise in pH value is not helpful for the materials to remove Cr(VI) from solutions. For Cr(VI) removal, the optimum pH value is 2. The adsorption of Cr(VI) by AC and ACI followed the pseudo-second-order kinetic model and Langmuir isothermal adsorption equation. The maximum adsorption value of Cr(VI) is 154.56 mg/g for AC and 241.55 mg/g for ACI. There is chemical adsorption during the Cr(VI) removal. A lot of Cr (III) was formed by Cr(VI). The abundance of pores and the reducing ability of the materials are essential for the removal of Cr (VI).

1. Introduction

Chromium is broadly utilized in several commercial strategies, including cloth manufacturing, metallic finishing, metallurgy, chrome electroplating, glassmaking, wood preservative, and the ceramic industry [49]. The discharge of wastewater containing chromium may contaminate water bodies and soil [44]. There are two typical species for Cr in natural ecosystems, separately Cr(III) and Cr(VI). There is a great toxicity for Cr(VI), because of strong solubility and significant oxidation propensity [1,45]. Due to Cr(VI) contamination, “cancer villages” appeared in some regions [21].

Currently, there are numerous methods to clean up Cr(VI) contamination from wastewater, including bioremediation [46], precipitation [3], photocatalytic reduction [31] , membrane treatment [21], oxidation filtration [63], electrochemical [33] and adsorption methods [10,12,53,55]. However, it was found that some treatment methods were pricy, challenging, and also produced dangerous secondary contaminants [40,66]. Adsorption has been called the most promising and well-liked treatment strategy because of its accessibility, improved removal effectiveness, and generally straightforward operation [47]. Adsorbents commonly used include

* Corresponding author. College of Chemistry and Chemical Engineering, Yulin University, Chongwen Road No.51, Yulin City, 719000, Shaanxi Province, China.
E-mail address: 99452715@qq.com (H. Wang).

https://doi.org/10.1016/j.heliyon.2023.e13267
Received 14 October 2022; Received in revised form 5 January 2023; Accepted 24 January 2023
Available online 26 January 2023

zeolite, molecular sieves, cellulose, montmorillonite, resins, carbon nanotubes, nanoparticles, nanocomposites, and activated carbon [15,23,64]. Because excellent properties are associated with activated carbon, such as low-cost raw materials, a simple production process, an abundance of pores, a large specific surface area, and excessive chemical stability and non-toxicity [18,52,59]. More and more research attention has focused on the application of biomass-activated carbon for removing Cr (VI) [52]. Many researchers have used activated carbon to remove Cr(VI) with excellent results [24]. For example, the granular activated carbon prepared from coconut shell presents excellent hexavalent chromium removal capability because of a high specific surface area, surface functional groups, and electron donors to convert Cr(VI) to Cr(III) [15].

Over the years, research has concentrated on the use of inexpensive raw materials to create a more effective activated carbon adsorbent for removing Cr (VI), such as wood [15], fruit shell [16], coconut shell [16], etc. Although activated carbon can be made from coal, biomass, and any carbon-rich waste. Renewable biomass was regarded as an ideal precursor-material for activated carbon with a large surface area [7]. It is a sensible measure to use waste biomass to produce activated carbon. Firstly, the carbon in biomass can be fixed, which stops CH_4 or CO_2 generation. Secondly, activated carbon, with a better value and less impact on the environment can be produced from biomass [34]. By-products from the biomass production and processing industry that are readily available and reasonably priced have shown to be suitable raw materials for the synthesis of activated carbons [67]. Precursor materials made from wood waste and sawdust are widely available and plentiful [15]. In addition to increasing the value of wood waste, it also expands the markets for the waste products produced by wood farmers and tackles the issue of waste management. So wood waste and sawdust have been extensively used to produce activated carbons. There is a large amount of wood-based activated carbon on the market. The method of preparation and chemical composition of wood species biomass are known to affect the adsorption characteristics of activated carbon [7,34,35]. So, it is necessary to provide further information regarding the relationship between the properties of activated carbon and the removal of hexavalent chromium.

At this point, we would like to call attention to a few key features that can help customers choose a woody-activated carbon that is more effective and reasonably priced for Cr(VI) removal from wastewater. For this paper, two kinds of wood-activated carbon powder from different manufacturers were chosen. The relationship between the properties of activated carbon and the removal of Cr(VI) was investigated, and the adsorption mechanism of Cr(VI) was looked at using the physicochemical properties of two activated carbons and a chromium adsorption experiment. The results provide theoretical support for the choice to employ woody-activated carbon in the chromium wastewater treatment process.

2. Materials and methods

2.1. Materials

The two kinds of woody-activated carbon powder were purchased respectively from different shops in Taobao. AC is from Longxin Water Purification Material Shop in Gongyi City. While ACI is from Hongshu Environmental Protection Factory Shop. ACI is physically activated, as opposed to AC, which is activated chemically. They are made using different production techniques. Hydrochloric acid (HCl), potassium dichromate ($K_2Cr_2O_7$), sodium hydroxide (NaOH), and other reagents used were analytical grade and made by Shanghai Sinopharm Group. In the experiment, deionized water was used.

2.2. The characterization of samples

SIGMA 300 FESEM made in Germany was employed to study the surface morphologies of the materials. Bruker TENSOR 27 FTIR made in Germany was used to determine the functional groups of adsorbents. The primary elemental composition of both materials was analyzed using an Elementar Vario EL Cube elemental analyzer manufactured in Germany. Elemental oxygen content was estimated by subtracting C, N, S, and H. Surface area, the volume of pores, and distribution of pore sizes of the samples were evaluated using an automatic specific surface area tester (ASAP 260, Micromeritics Instrument Corp, USA). Using Thermo Scientific™ K-Alpha™ XPS, the changes in elemental composition and the functional groups of the material surface after the adsorption were obtained. The pH meter (PHS–3C, Shanghai Lei Magnetic) was calibrated before each usage and then was used to determine the pH level of the solution. Iodine levels for the two materials were calculated individually using the China national standard method (GB/T 1296.8–2015). The concentration of oxygen-containing functional groups on the sample surface was determined using Boehm titration method [41]. In this paper, the point of zero electric charge (pH_{pzc}) was measured using the pH drift method [43].

2.3. Estimating removal capability of Cr(VI)

A batch of adsorption experiments was carried out. In centrifugal tubes, 0.05 g of material was mixed in 50 ml of Cr(VI)-containing simulated wastewater for 24 h at room temperature and 150 rpm. In order to carry out a kinetic study, at Cr(VI) initial concentration of 100 mg/L and pH 2.0, adsorption kinetic was studied by measuring the amount of Cr(VI) residue at different reaction times (0.5–96 h). The relationship between pH in the range of 1.0–6.0 and the Cr(VI) removal amount was observed. The pH levels were adjusted with NaOH at 0.05 mol/L and HNO_3 at 0.05 mol/L. When the initial concentration of Cr(VI) was in the range of 10–600 mg/L, at room temperature and pH 2.0, Cr(VI) adsorption isotherms were studied. 1, 5 - Diphenylcarbohydrazide spectrophotometric technique was used to determine the amounts of Cr(VI) with a UV–vis spectrophotometer (UV1800, Shimadzu, Japan). A suitable sample of transparent water (less than 50 g of hexavalent chromium) was put in a 50 ml colorimetric tube, and diluted with water to the standard line. Shake thoroughly after adding 0.5 ml of each phosphoric and sulfuric acid solution, and 2 ml of color developer. After 10 min, the

hexavalent chromium content was determined from the calibration curve by using a 10 mm cuvette with water as a reference at 540 nm to determine the absorbance.

To calculate the removal effectiveness (R) and equilibrium adsorption quantity (q_e) of Cr(VI), Eq. (1) [13] and Eq. (2) [11] were utilized.

$$R = \frac{C_0 - C_e}{C_0} \times 100\% \tag{1}$$

$$q_e = \frac{(C_0 - C_e) \times V}{m} \tag{2}$$

where V (L) is the volume of solution; m (g) signifies the amount of the prepared samples; C_0 (mg/L) is the initial concentration of Cr (VI), and C_e (mg/L) is the equilibrium concentration of Cr(VI).

2.4. Adsorption kinetics analysis

To evaluate the adsorption principle of the samples on Cr(VI), the adsorption dynamics of the materials were carefully examined by the pseudo–first-order kinetic model, pseudo–second- order kinetic model, intra-particle diffusion model, modified Freundlich model, Elovich model, and film diffusion model. Eqs. (3)–(3)–(9) are the formulas and variables for the six kinetic models:

Pseudo-first-order model (PFO) [41]:

$$\ln(q_e - q_t) = \ln q_e - k_1 t \tag{3}$$

Pseudo-second-order model (PSO) [41]:

$$\frac{\mathrm{t}}{q_t} = \frac{1}{k_2 q_e^2} + \frac{t}{q_e} \tag{4}$$

Intra-particle diffusion model (IPD) [32]:

$$q_t = k_d t^{0.5} \tag{5}$$

$$q_t = k_d t^{0.5} + C \tag{6}$$

Elovich model [9]:

$$\mathrm{q_t} = \frac{1}{\beta}\ln(\alpha\beta) + \frac{1}{\beta}\ln t \tag{7}$$

Modified Freundlich model (MF) ([65]:

$$\ln(q_t) = A + B \times \ln(t) \tag{8}$$

Liquid-film diffusion model (LFD) [43]:

$$\ln\left(1 - \frac{q_t}{q_e}\right) = -k_f \times t \tag{9}$$

The adsorption time is expressed by t; q_t is the amount of adsorption at time t; q_e is the equilibrium adsorption volume. The rate constants are k_1 for PFD, k_2 for PSD, k_d for IPD, and k_f for LFD; A, B, C, α, and β, respectively, are the dynamic constants of the various models.

2.5. Adsorption isotherm model

To understand the adsorption process and look at how samples and Cr(VI) interact, some isotherm models were adopted. Data from the adsorption experiment was collected and fitted using the four adsorption isotherm models. Eqs. (10)–(15) are the formulas and variables:

Langmuir isotherm model [9]:

$$\frac{C_e}{q_e} = \frac{C_e}{q_m} + \frac{1}{q_m K_L} \tag{10}$$

Freundlich isotherm model [37]:

$$\ln q_e = \ln K_F + \frac{1}{n}\ln C_e \tag{11}$$

Temkin isotherm model [37]:

$$q_e = \frac{RT}{b_T}\ln k_T + \frac{RT}{b_T}\ln C_e \tag{12}$$

Dubinin - Radushkevich isotherm model [20]:

$$\ln q_e = \ln q_m - \beta \times \varepsilon^2 \tag{13}$$

$$\varepsilon = RT \ln\left(1 + \frac{1}{C_e}\right) \tag{14}$$

$$E_a = \frac{1}{\sqrt{2 \times \beta}} \tag{15}$$

The following parameters: Cr(VI) equilibrium concentration to C_e (mg/L); the highest fitted adsorption amount to q_m (mg/g); Langmuir constant to k_L (L/mg); Freundlich constant to K_F((mg/g)/(L/mg)$^{1/n}$); the empirical parameters to n; Temkin constant to k_T (L/mg); Dubinin- Radushkevich constant to β (mol^2/kJ^2).

3. Results and discussion

3.1. Characterization

3.1.1. Physicochemical properties

Characteristic parameter of AC and ACI are listed in Table 1. It can be found that the atomic percentages of N, C, and S in AC are obviously higher than that in ACI, while O and H are the opposite. There are high C of concentration for AC, indicating that AC has high carbonization. ACI contains more carboxyl and lactonic groups than AC, but the phenolic hydroxyl groups are the exact opposite. It was revealed that the makeup of the surface functional groups of the two materials varied significantly. ACI has a higher ratio of H/C, (N + O)/C, and O/C, indicating that ACI is more polar, aromatic, and hydrophilic [2,6]. The iodine sorption value of ACI is 1276 mg/g. It is higher than AC, indicating that ACI has a more big specific surface area [8]. In general, materials with more oxygen functional groups, strong polarity, and a big surface area are regarded as good adsorbent for contaminant removal [25].

3.1.2. The porous texture of the materials

The pore diameters distribution and specific surface area of the materials were identified using a nitrogen adsorption experiment. As shown in Fig. 1 (a), the isotherms of the two materials abruptly increased at relative pressures below 0.1, indicating the presence of significant numbers of micropore structures in the materials [57]. Additionally, both showed pronounced hysteresis loops at 0.5 relative pressure, proving that there are intermediate pores in the materials [29]. It can be classified as the combined type I/IV isotherms according to IUPAC classification [48]. Thus, a mesopore and micropore combination structure were visible in the two materials. Additionally, ACI has a higher isothermal adsorption curve than AC, indicating that ACI has a rich porous structure and a large specific surface area.

Micropores are concentrated in the range of 0.5–2 nm, whereas mesopores are concentrated in the range of 2–50 nm. Fig. 1 (b) demonstrates that ACI contains significantly more micropores and mesopores than AC. According to the isotherm of nitrogen adsorption/desorption, the relevant textural parameters of the samples were calculated. Table 2 provides a summary of the outcome. It has been discovered that ACI has a larger surface area, a higher volume of micropores, and a bigger average pore diameter than AC. This is in line with the results of the iodine sorption value comparison, which show that ACI has a higher iodine level than AC and a greater abundance of micropore structure [31]. ACI with well-developed porosity is likely to have better adsorption capacity for Cr(VI) in water solution.

FESEM was used to observe the microscopic morphology of the materials. In AC, a comparatively porous, smooth structure was found, as shown in Fig. 2(a) and (b). ACI shows a coarse surface with a truly rich pore structure in Fig. 2(c) and (d). Compared with AC, ACI displayed more nanopores, which agreed with its high pore volume and large surface area.

3.1.3. Surface properties

At 400 to 4000 cm^{-1} wavenumber, the FTIR spectra of both materials were obtained. Oxygen-containing functional groups, which play an important role in the removal of Cr(VI) [56,61], were found on the surface of the materials. At wavenumber of 3429 cm^{-1}, O–H groups were found in Fig. 3. Other peaks belong to the following: (a) 2848 cm^{-1} and 2923 cm^{-1} to symmetry and asymmetry of alkyl –CH_2 [36]; (b) 1600 cm^{-1} to conjugated ketones and quinones C═O stretching or aromatic C═C stretching [38]; (c) 1382 cm^{-1} to

Table 1
Physicochemical properties of the two materials.

Samples	Ultimate analysis (dry ash free, wt. %)					Atomic ration (%)			Acidic groups (mmol/g)			Iodine number (mg/g)
	C	H	O	N	S	H/C	(N + O)/C	O/C	Carboxylic	Lactonic	Phenolic	
AC	86.33	1.84	11.01	0.70	0.12	0.021	13.55	0.13	0.56	0.24	0.16	1145
ACI	81.11	2.33	15.97	0.58	0.11	0.029	20.40	0.20	0.84	0.56	0.12	1276

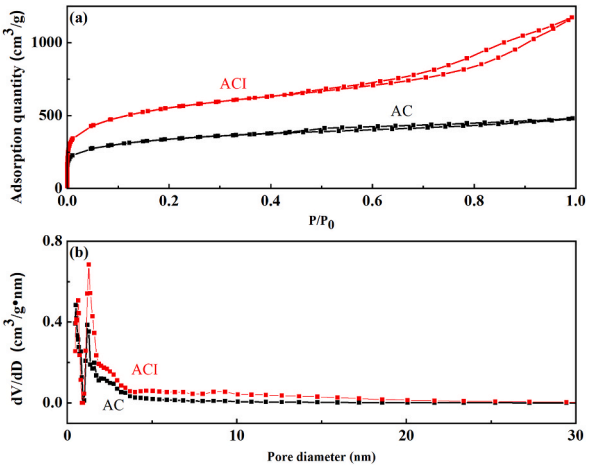

Fig. 1. (a) Nitrogen absorption-desorption isotherm, and (b) pore distribution of the two materials.

Table 2
The pore structure parameters of the two samples.

Samples	Surface area (m^2/g)	t-Plot Micropore area (m^2/g)	t-Plot external surface area (m^2/g)	Total pore volume (mL/g)	t-Plot micropore volume (mL/g)	Average pore diameter (nm)
AC	1197.81	497.29	700.51	0.7203	0.2128	2.4054
ACI	1928.11	616.36	1311.75	1.6781	0.2758	3.4814

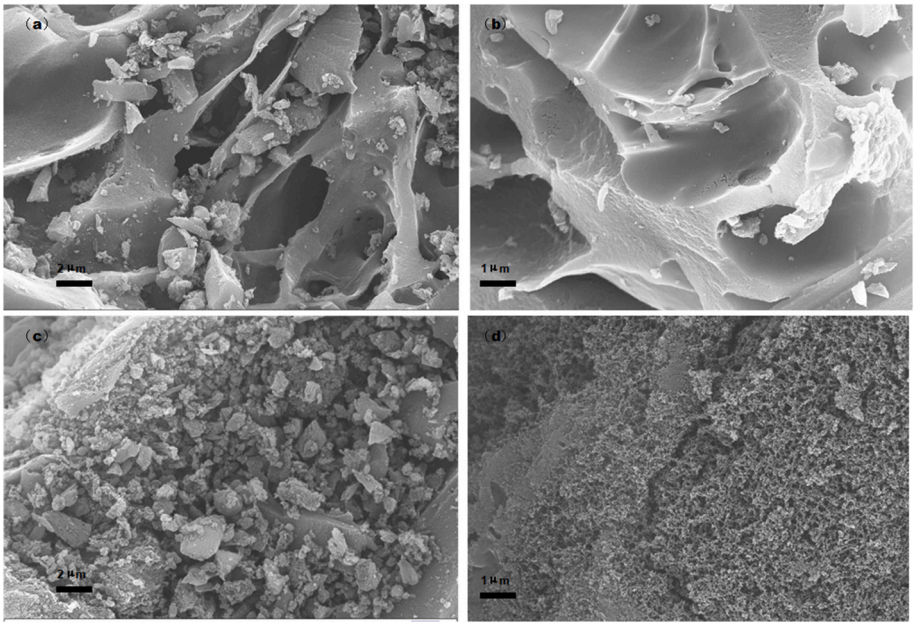

Fig. 2. SEM image of the two materials (a) × 5000 for AC, (b) × 10,000 for AC, (c) × 5000 for ACI, and (d) × 10,000 for ACI.

ester groups and carboxyl [62]; (d) 1120 cm^{-1} to ether group, phenol group, the ester group or alcohol group of C–O stretching vibration on material of surface [54]; (e) 876 cm^{-1} to aromatic out of plane deformation of C–H bending [38,50], and (f) 617 cm^{-1} to the stretching of inorganic moieties [26,51].

The peaks of C–O stretching vibration of AC showed more intensity than ACI, while C═O stretching and aromatic C═C stretching were on the contrary. When the materials were adsorbed by Cr(VI), some groups, such as O–H, C═O/O–C–O, and -O-C═O, showed a peak shift or intensity change in Fig. 3. There are clear weakening peaks around 1120 cm^{-1}. There are noticeably growing peaks at 1600 and 1382 cm^{-1}. It implied that the oxygen-containing functional groups are closely related to Cr(VI) removal.

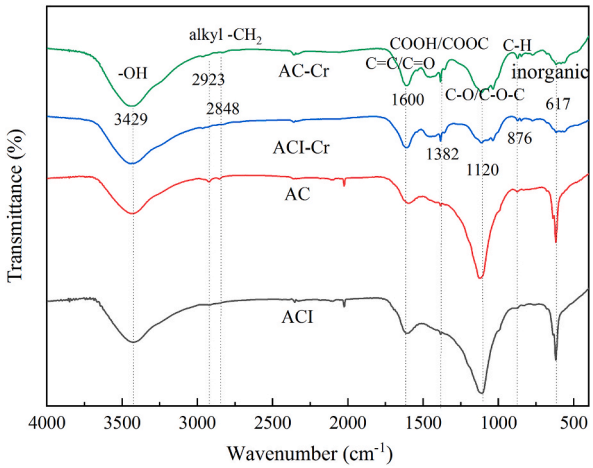

Fig. 3. FTIR spectra of the two materials before and after Cr(VI) adsorbtion.

3.2. Adsorption characteristics

3.2.1. Comparison of adsorption capacity

Fig. 4(a) shows the evaluation of the two materials' capacity to remove Cr(VI). It is evident that 71.79% of Cr(VI) was removed

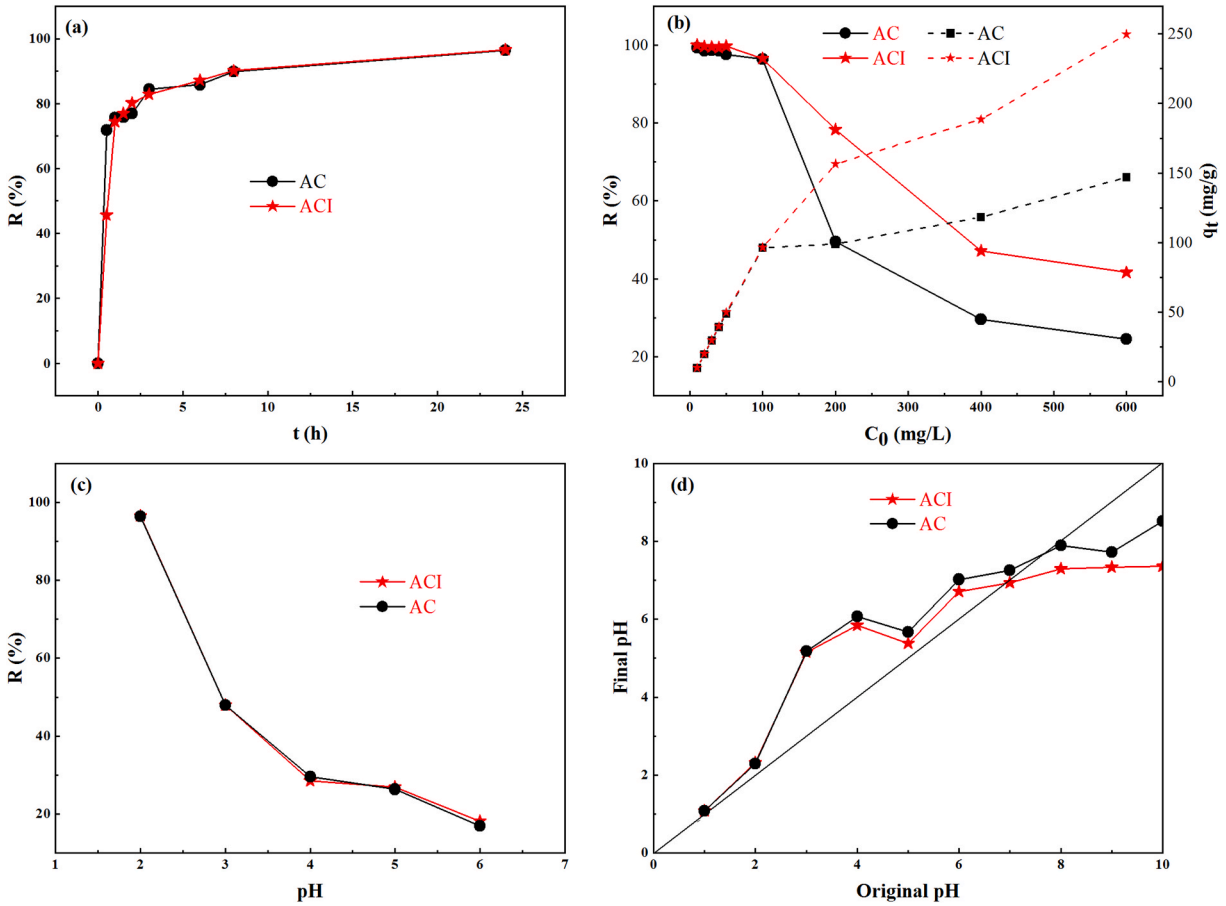

Fig. 4. (a) Comparison of the two materials' Cr(VI) removal rates at various reaction times, (b) comparison of the two materials' Cr(VI) adsorption capacities and removal rates at various starting concentrations, (c) comparison of the two materials' Cr(VI) removal rates at various pH levels; and (d) determination of point of zero charge of the two materials by pH drift method.

from the solution by AC at 30 min, which is 1.5 times that of ACI. The removal rate of hexavalent chromium by ACI increased rapidly and was comparable to AC at 1 h of adsorption and exceeded AC after 6 h. The different surface areas, pore sizes, and functional groups between AC and ACI may be the cause of this discrepancy.

3.2.2. The relationship between the initial concentration and Cr(VI) removal

The removal rate of Cr(VI) and the adsorption capacity of AC and ACI at various starting concentrations are displayed in Fig. 4(b). As the initial concentration rises, the removal rate gradually declines, while AC and ACI's adsorption capacity steadily rises. When the initial concentration is below 100 mg/L, more than 95% of Cr(VI) is removed by the two materials. But when the initial concentration increases from 100 mg/L to 600 mg/L, the removal percentage of Cr(VI) decreases to 24.5% for AC and 41.6% for ACI. The adsorption capacity always increases as the initial concentration increases. But, when the initial concentration is above 100 mg/L, the increased rate of adsorption capacity obviously decreases, especially for AC, indicating the reduction of active sites and a greater amount of chromium layer covering the sample surface. When the concentration of Cr(VI) exceeds 100 mg/L, the two materials used in this study have various degrees of Cr(VI) removal capability. Compared to AC, ACI is more suitable for treating wastewater with high Cr(VI) content.

3.2.3. The relationship between pH value and Cr(VI) removal

It can be shown in Fig. 4(c) that the value of solution pH has a substantial impact on the ability of two materials to remove Cr(VI). The removal effectiveness started to decline quickly (pH 2–4), then declined slowly (pH 4–6) as the solution pH levels rose. Both materials displayed the maximum clearance rates at a pH value of 2. The ideal reaction conditions for eliminating Cr(VI) were at pH 2. It is consistent with earlier studies [49]. The surface properties of the materials and the present species of chromium at various pH levels may be related to Cr(VI) removal.

For Cr(VI), the species, such as Cr_2O_7、$HCrO^-$、$Cr_3O_{10}^{2-}$ and CrO_{13}^{2-} were stable in solution [28]. The predominant species of Cr(VI) at low pH values was $HCrO^-$, while CrO^{2-} was the primary formation in the solution at a high pH value [5,26]. Fig. 4(d) demonstrates that the pH_{pzc} of AC (7.67) and ACI (6.91) were higher than pH 6. When pH < pH_{pzc}, the samples' surface functional groupings were protonated by the high concentration of H^+, giving them positive charges. This is advantageous for the adsorption of anionic $HCrO^-$. When pH > pH_{pzc}, as the amount of OH^- rose in the alkaline environment, the surface of the materials developed a stronger negative charge. This prevented samples from adsorbing chromium ions by electrostatic interaction. According to these, in acidic solutions Cr

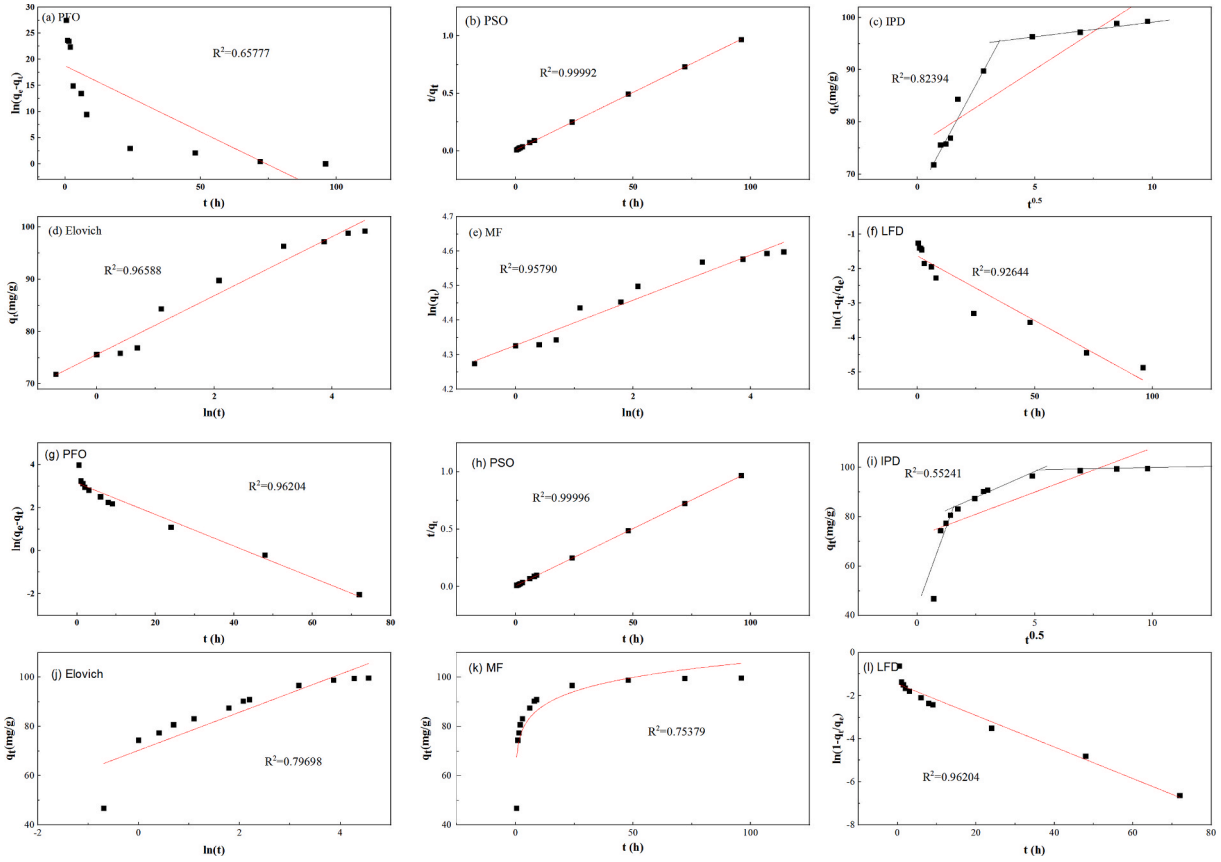

Fig. 5. Adsorption kinetics fitted models of Cr(VI) by the two materials, (a)–(f) for AC, and (g)–(l) for ACI.

(VI) of adsorption may have been facilitated by electrostatic contact, but in alkaline solutions, ion exchange appears to have been the dominant process [27]. Additionally, other studies have shown that strong acidic conditions is helpful to the conversion of Cr(VI) to Cr (III) [27].

3.3. Adsorption kinetics analysis

Dynamics analysis can offer a solid foundation for the forecasting of adsorption behavior. By kinetic models, the adsorption mechanism can be revealed, and adsorption resistance can be obtained. Six kinetic models were used to analyze the samples' adsorption behavior on Cr(VI). The fitting of Cr(VI) adsorption kinetic by various models is depicted in Fig. 5. The evaluated kinetic fitting parameters are listed in Table 3. The best model for the adsorption process is chosen using the correlation coefficient.

It was found that PSO, Elocich, and MF models for AC, and PFO, PSO, and LFD models for ACI can reproduce the kinetic data with R^2 higher than 0.95. However, there is a marked difference between the equilibrium capacity calculated with the PFO model for ACI and the value of the experiment. So, the adsorption of Cr(VI) on ACI can be more precisely described using the PSO kinetic model. For AC and ACI, the correlation coefficient of the PSO model was the highest ($R^2 > 09999$), indicating that the PSO model can be used to better demonstrate how Cr(VI) is removed. This result was consistent with other research on biochar to remove Cr(VI) [39].

Moreover, the removal capacity of the two materials obtained by the PSO kinetic model matched the outcomes of the trial. This further confirms that PSO kinetic was credible in analyzing the procedure for Cr(VI) removal. The PSO model claims that this process is chemical adsorption [39]. In this adsorption procedure, the adsorbent and the adsorbent share or transfer electrons [19,42]. Accordingly, the most probable method for removing Cr(VI) was chemical adsorption, which involves valency forces via the transfer of electrons between chromium and material [19]. The kinetic data obtained from PSO and Elovich model for AC demonstrates that the number of active sites mainly controls the Cr(VI) adsorption rate [53].

3.4. Adsorption isotherm analysis

When the adsorption reaches its end, the interface of the two phases achieves equilibrium. The relationship between the two phases is described by the equilibrium curve. This equilibrium curve is the adsorption isotherm. It can reveal the surface and pore properties of the samples. Four isotherm models were used to replicate the two materials' adsorption abilities for Cr(VI) removal in order to better understand their behavior and surface makeup. The fitting results are displayed in Fig. 6. Table 4 provides a summary of the corresponding parameters. The Langmuir isotherm was the optimal model that fits the experiment's results, with the highest correlation coefficients for the two materials among the four models. This indicates that two materials with a homogenous monolayer surface have energetically equal active sites that interact with Cr(VI). K_L is the Langmuir constant, which has to do with the bonding site's affinity and adsorption energy [1]. By calculations, the values of K_L for AC and ACI were 1.151 L/mg and 0.1368 L/mg, respectively. This suggests that the relationship between the two materials and Cr(VI) was a favorable adsorption process [4,14,30]. According to the Langmuir model, the greatest Cr(VI) adsorption amounts for AC and ACI, respectively, were 154.56 mg/g and 241.55 mg/g. For ACI and AC, the Temkin model is also suitable because of its high correlation coefficient. The adsorption of Cr(VI) onto ACI can also be successfully fit using the Freundlich model. The Freundlich model parameter values n were higher than 1, suggesting favorable adsorption conditions for ACI [60].

3.5. Adsorption mechanism

The chemical structure of the adsorbent surface and the valence change of elements were examined using XPS. This can be better

Table 3
List of parameters of various kinetic models that account for Cr(VI) removal by the two materials.

Kinetic models	Parameters	AC	ACI
PFO	K_1 ($L\ h^{-1}$)	0.2528	0.07317
	q_e ($mg\ g^{-1}$)	1.3965×10^8	23.2023
	R^2	0.65777	0.96204
PSO	K_2 ($g\ mg^{-1}\ h^{-1}$)	0.01626	0.015091
	q_e ($mg\ g^{-1}$)	99.6016	100.2004
	R^2	0.99992	0.99996
IPD	K_d ($mg\ g^{-1}\ h^{-0.5}$)	14.8635	15.4220
	R^2	0.8294	0.55241
Elovich	α($mg\ g^{-1}\ h^{-1}$)	3.7929×10^6	6.9069×10^4
	β ($g\ mg^{-1}$)	0.1775	0.1294
	R^2	0.96588	0.79698
MF	A	0.0655	4.2331
	B	4.3269	0.1006
	R^2	0.95790	0.75379
FD	K_f	0.06219	0.1040
	q_e ($mg\ g^{-1}$)	99.24	99.59
	R^2	0.92644	0.96204

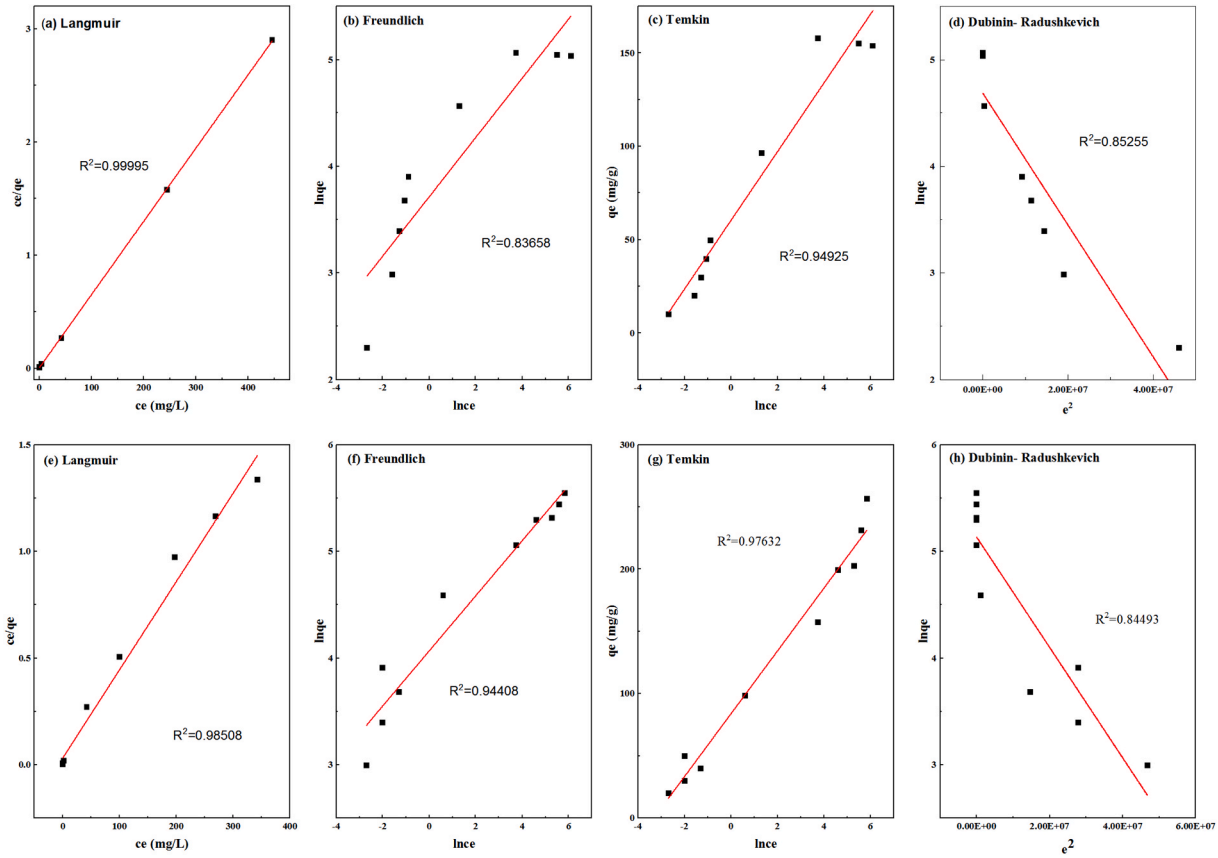

Fig. 6. Adsorption isotherms fitted models of Cr(VI) by the two materials, (a)–(d) for AC, and (e)–(h) for ACI.

Table 4
List of parameters for two materials' isothermal adsorption models.

Isotherm models	Parameters	Adsorbent	
		AC	ACI
Langmuir	q_m (mg/g)	154.56	241.55
	K_L (L/mg)	1.151	0.1368
	R^2	0.99995	0.98508
Freundlich	$K_F((mg/g)/(L/mg)^{1/n})$	40.981	58.326
	N	3.600	3.873
	R^2	0.83658	0.94408
Temkin	b_T (KJ/mol)	134.717	98.241
	K_T (L/mg)	26.549	27.799
	R^2	0.94925	0.97632
Dubinin − Radushkevich	q_m (mg/g)	108.582	169.837
	$\beta(mol^2/kJ^2)$	6.181×10^{-8}	5.174×10^{-8}
	E_a (kJ/mol)	2844.11	3108.65
	R^2	0.85255	0.84493

understand the two materials' possible ability to remove Cr(VI). The results are shown in Fig. 7. Each element's peak area and relative atomic content were analyzed. Table 5 provides a list of the values. As seen in Fig. 7 (a) and (b), prior to the adsorption of Cr(VI), C and O make up the majority of the surface elements on AC and ACI. Following the adsorption of Cr(VI), the O1s peak's intensity significantly increased, and a new Cr 2p peak emerged. The fact that Cr 2p peak emerged was proved that the surface of AC and ACI successfully adsorbed Cr(VI). The values of O/C go down by 0.067 for AC and 0.109 for ACI. It can be inferred that there were chemical reactions during the adsorption process. The same results were found in other research [22].

The C1s spectra of the materials before and after adsorption of Cr(VI) was compared, as seen in Fig. 8 (a) and (b). The high-resolution C1s peak can be divided into four peaks [22]. As shown in Fig. 8, the distinct peaks attributed to phenols, alcohols, or ether-based C–O functional groups decreased from 35.03% to 7.58% for AC and from 12.21% to 6.32% for ACI after the adsorption of

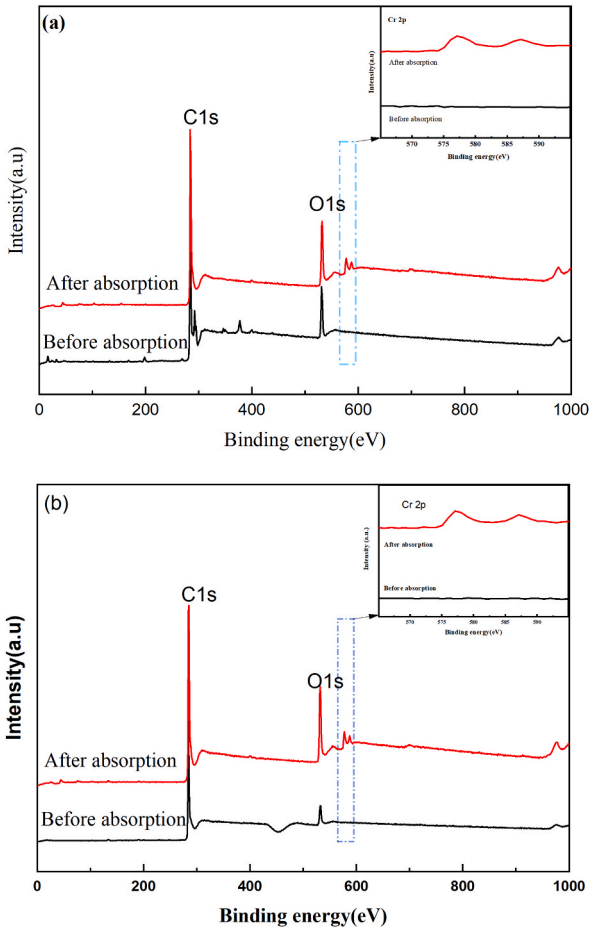

Fig. 7. XPS spectra of the two materials before and after Cr(VI) adsorbtion, (a) AC; and (b) ACI.

Table 5
Atomic percentage of the two materials' surface before and after adsorption of Cr (VI).

Form	Atomic percentage (%)			
Elements	AC	AC-Cr	ACI	ACI-Cr
C (%)	89.07	82.68	91.22	81.66
O (%)	10.93	15.74	8.78	16.77
Cr (%)	0.00	1.57	0.00	1.56
O/C	0.123	0.190	0.0963	0.205

Cr(VI), respectively. At the same time, C═O functional groups increased from 4.50% to 15.24% for AC and from 8.30% to 15.75% for ACI after the adsorption of Cr(VI), respectively. This behavior could be the result of a chemical redox reaction. When Cr(VI) was adsorbed on the samples, a part of C–O oxidized to C═O.

This speculation is further confirmed by the following phenomenon. The high-resolution O1s peak can be divided into three peaks [58]. In the O 1s XPS spectra (Fig. 9 (a) and (b)), the characteristic peaks value of C–OH obviously decreased from 72.12% to 52.13% for AC and from 66.66% to 43.83% for ACI after Cr(VI) removal, respectively. In contrast, the peak value of O–C═O rose from 13.90 to 34.61% for AC and from 6.91% to 35.03% for ACI, respectively. These are in accord with the above C1s fitting results. These observations suggest that during the removal of Cr(VI), C–OH, -O-C═O, C–O, and C═O functional groups play a significant influence. The outcomes of earlier FTIR analyses also support this.

The redox reaction between C–O and Cr(VI) may be the cause of the ratio of C–O decreasing. C–O may be the electron-donating groups of the materials and be oxidized to C═O or O–C═O with Cr(VI) adsorbing on the materials and partially changed to Cr(III), which was found at the split peaks of Cr 2p in Fig. 10 (a) and (b). The high-resolution Cr 2p peak can be divided into four peaks [17]. After Cr(VI) adsorption, Cr(III) was found on AC for 70.00% and on ACI for 73.73%, respectively, while Cr(VI) is only 30.00% for AC and 26.27% for ACI. There are more amounts of Cr(III) generation for ACI, which has better removal of Cr (VI). This supports the idea

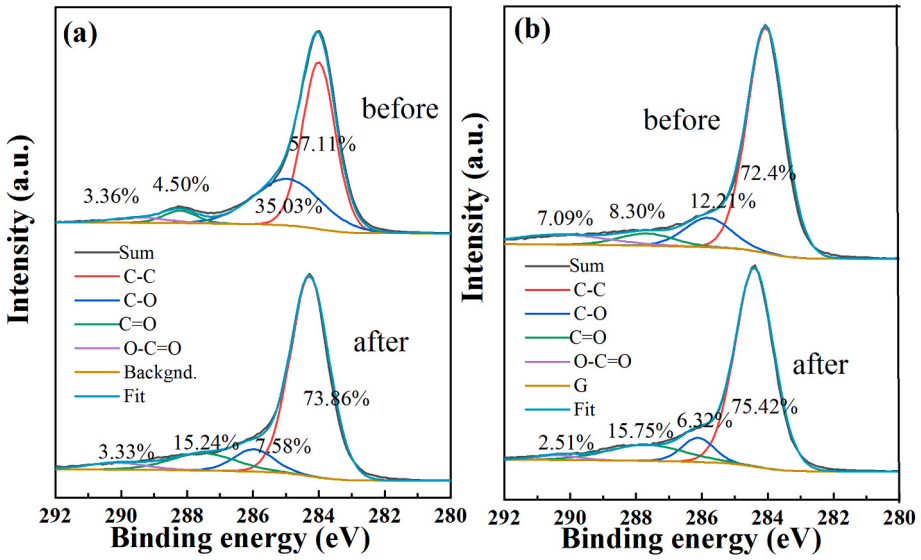

Fig. 8. C1s split peak fitting results of the two materials before and after Cr(VI) adsorbtion, (a) AC; and (b) ACI.

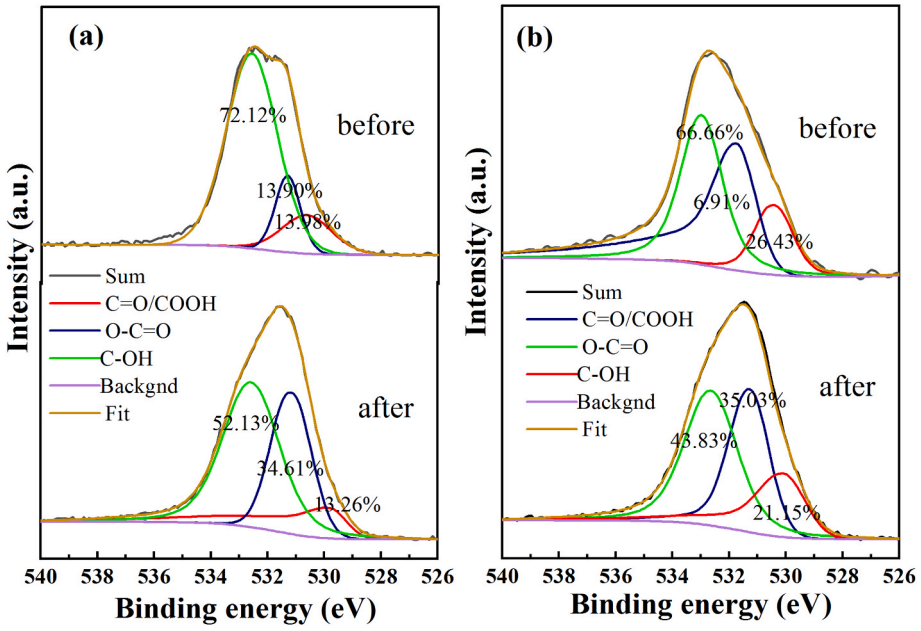

Fig. 9. O1s split peak fitting results of the two materials before and after Cr(VI) adsorbtion, (a) AC; and (b) ACI.

that redox processes are crucial to the elimination of Cr(VI). Additionally, it was speculated that interactions, including ion exchange, complexation, precipitation, and electrostatic attraction, may also contribute to the removal of Cr(VI) based on the adsorption variation trend on samples with pH values and the results from chromium adsorption isotherm and kinetic analysis.

According to these results, the Cr(VI) removal process by the AC and ACI can be summarized as follows: (1) the adsorbent has a rich porous structure and high specific surface area that provided enough loading sites for Cr(VI) by precipitation and electrostatic attraction; (2) many Cr(VI) ions are loaded on the surface of the material, which are then oxidized by C–O or other functional groups to form Cr(III); (3) Cr(III) formed by Cr(VI) was partially fixed on the materials, and the remainder could be dissolved in solution; (4) Cr (VI) that is not converted on the surface of the material, is retained by some means such as ion exchange, electrostatic adsorption or precipitation.

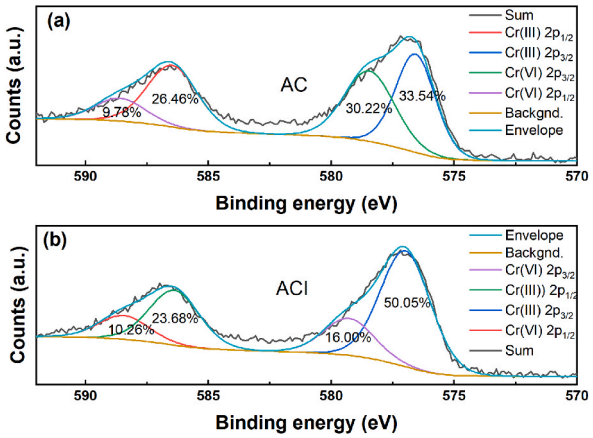

Fig. 10. Cr 2p split peak fitting results of the two materials after Cr(VI) adsorbtion, (a) AC; and (b) ACI.

4. Conclusion

In this paper, to remove Cr(VI) in solution, two types of woody activated carbon were utilized. The relationship between Cr(VI) removal rate and solution pH, as well as starting concentration, was studied. The removal mechanism of Cr(VI) was researched by a series of characterization means, with the adsorption isotherms and adsorption kinetic analysis.

ACI, with a higher proportion of oxygen-containing acid functional group, showed higher polarity, aromaticity, and iodine level than AC. Both materials are rich in micropores and mesopores and have a large specific surface area. ACI shows higher S_{BET} and average pore than AC. They display similar FTIR spectra and a similar change of peaks during Cr(VI) adsorption process. In the low concentration range, both exhibited good adsorption performance. When the concentration is above 100 mg/L, the difference among the samples is obvious, and ACI exhibits a greater ability to remove Cr(VI). As Cr(VI) concentration rose, the removal rate value dropped.

The elimination of Cr(VI) was significantly impacted by the pH value. The pH level of 2 was ideal for eliminating Cr(VI). As pH rose, the rate of Cr(VI) elimination decreased noticeably. Cr(VI) could be effectively removed from aqueous solutions using both materials. The PSO kinetics model can more accurately predict the kinetics of the removal of Cr(VI) for the materials than other kinetic models, suggesting that Cr(VI) removal is mostly a process of monolayer chemisorption. Compared with other adsorption isotherm modes, the experiment dates were well fit by the Langmuir isotherm, with the highest correlation coefficients. It indicates that the surface of the samples is uniform, and Cr(VI) adsorption occurs by a single layer of molecules.

The reduction function groups of the materials have a good role in the removal process of Cr(VI). After adsorption, Cr(III) predominated as the main form of chromium on the surfaces of the material. The Cr(VI) removal process is explained as follows. First, Cr (VI) was electrostatically attracted to or exchanged with the ions on the surface of the material. Second, the surface functional groups reduced the abundant portion of Cr(VI) to Cr(III). Finally, some Cr(III) was fixed in the materials through ion exchange or chelation, while the others may be released into the solution.

Author contribution statement

Hua Wang: Conceived and designed the experiments; Performed the experiments; Analyzed and interpreted the data; Contributed reagents, materials, analysis tools or data; Wrote the paper. Wencheng Wang; Song Zhou: Performed the experiments. Xuchun Gao: Analyzed and interpreted the data.

Funding statement

Miss Hua Wang was supported by Shaanxi Province Science and Technology Department Project [2020NY-165], Yulin Science and Technology Bureau [CXY202000503/CXY202000505], Yulin High-tech Zone Project [CXY202120/CXY202142], YLU-DNL Fund [2,022,010].

Data availability statement

Data included in article/supp. material/referenced in article.

Declaration of interest's statement

The authors declare no competing interests.

References

[1] A. Ashraf, I. Bibi, N.K. Niazi, Y.S. Ok, G. Murtaza, M. Shahid, A. Kunhikrishnan, D. Li, T. Mahmood, Chromium(VI) sorption efficiency of acid-activated banana peel over organo-montmorillonite in aqueous solutions, Int. J. Phytoremediation 19 (2017) 605–613.

[2] Z. Chang, L. Tian, J. Zhang, D. Zhou, Comparative study on the relative significance of low-/high-condensation aromatic moieties in biochar to organic contaminant sorption, Ecotoxicol. Environ. Saf. 238 (2022), 113598.

[3] Q. Chen, Y. Yao, X. Li, J. Lu, J. Zhou, Z. Huang, Comparison of heavy metal removals from aqueous solutions by chemical precipitation and characteristics of precipitates, J. Water Proc. Eng. 26 (2018) 289–300.

[4] Y. Chen, Y. Qian, J. Ma, M. Mao, L. Qian, D. An, New insights into the cooperative adsorption behavior of Cr(VI) and humic acid in water by powdered activated carbon, Sci. Total Environ. 817 (2022), 153081.

[5] Y. Chen, B. Wang, J. Xin, P. Sun, D. Wu, Adsorption behavior and mechanism of Cr(VI) by modified biochar derived from Enteromorpha prolifera, Ecotoxicol. Environ. Saf. 164 (2018) 440–447.

[6] W.Y. Cheng, F.Y. Li, J.H. Lv, M.X. Lin, W. W, Sorption characteristics of polycyclic aromatic hydrocarbons phenanthrene on sunflower straw biochar modified with alkali, Ecol. Environ. Sci. 31 (2022) 824–834.

[7] M. Danish, T. Ahmad, A review on utilization of wood biomass as a sustainable precursor for activated carbon production and application, Renew. Sustain. Energy Rev. 87 (2018) 1–21.

[8] M. Del Bubba, B. Anichini, Z. Bakari, M.C. Bruzzoniti, R. Camisa, C. Caprini, L. Checchini, D. Fibbi, A. El Ghadraoui, F. Liguori, S. Orlandini, Physicochemical properties and sorption capacities of sawdust-based biochars and commercial activated carbons towards ethoxylated alkylphenols and their phenolic metabolites in effluent wastewater from a textile district, Sci. Total Environ. 708 (2020) 135–217.

[9] T.C. Egbosiuba, A.S. Abdulkareem, A.S. Kovo, E.A. Afolabi, J.O. Tijani, M. Auta, W.D. Roos, Ultrasonic enhanced adsorption of methylene blue onto the optimized surface area of activated carbon: adsorption isotherm, kinetics and thermodynamics, Chem. Eng. Res. Des. 153 (2020) 315–336.

[10] T.C. Egbosiuba, A.S. Abdulkareem, A.S. Kovo, E.A. Afolabi, J.O. Tijani, M.T. Bankole, S. Bo, W.D. Roos, Adsorption of Cr(VI), Ni(II), Fe(II) and Cd(II) ions by KIAgNPs decorated MWCNTs in a batch and fixed bed process, Sci. Rep. 11 (2021) 75.

[11] T.C. Egbosiuba, A.S. Abdulkareem, A.S. Kovo, E.A. Afolabi, J.O. Tijani, W.D. Roos, Enhanced adsorption of As(V) and Mn(VII) from industrial wastewater using multi-walled carbon nanotubes and carboxylated multi-walled carbon nanotubes, Chemosphere 254 (2020), 126780.

[12] T.C. Egbosiuba, A.S. Abdulkareem, J.O. Tijani, J.I. Ani, V. Krikstolaityte, M. Srinivasan, A. Veksha, G. Lisak, Taguchi optimization design of diameter-controlled synthesis of multi walled carbon nanotubes for the adsorption of Pb(II) and Ni(II) from chemical industry wastewater, Chemosphere 266 (2021), 128937.

[13] T.C. Egbosiuba, M.C. Egwunyenga, J.O. Tijani, S. Mustapha, A.S. Abdulkareem, A.S. Kovo, V. Krikstolaityte, A. Veksha, M. Wagner, G. Lisak, Activated multi-walled carbon nanotubes decorated with zero valent nickel nanoparticles for arsenic, cadmium and lead adsorption from wastewater in a batch and continuous flow modes, J. Hazard Mater. 423 (2022), 126993.

[14] Y. Fang, J. Wen, G. Zeng, F. Jia, S. Zhang, Z. Peng, H. Zhang, Effect of mineralizing agents on the adsorption performance of metal-organic framework MIL-100 (Fe) towards chromium(VI), Chem. Eng. J. 337 (2018) 532–540.

[15] Y. Fang, K. Yang, Y. Zhang, C. Peng, A. Robledo-Cabrera, A. López-Valdivieso, Highly surface activated carbon to remove Cr(VI) from aqueous solution with adsorbent recycling, Environ. Res. 197 (2021), 111151.

[16] R. Gottipati, S. Mishra, Preparation of microporous activated carbon from Aegle Marmelos fruit shell and its application in removal of chromium(VI) from aqueous phase, J. Ind. Eng. Chem. 36 (2016) 355–363.

[17] Y. He, J. Chen, J. Lv, Y. Huang, S. Zhou, W. Li, Y. Li, F. Chang, H. Zhang, T. Wågberg, G. Hu, Separable amino-functionalized biochar/alginate beads for efficient removal of Cr(VI) from original electroplating wastewater at room temperature, J. Clean. Prod. 373 (2022) 133–790.

[18] A.M. Herrera-González, M. Caldera-Villalobos, A.-A. Peláez-Cid, Adsorption of textile dyes using an activated carbon and crosslinked polyvinyl phosphonic acid composite, J. Environ. Manag. 234 (2019) 237–244.

[19] Y.S. Ho, J.C.Y. Ng, G. McKay, Kinetics of pollutant sorption by biosorbents: Review, Separ. Purif. Methods 29 (2000) 189–232.

[20] Q. Hu, Z. Zhang, Application of Dubinin–Radushkevich isotherm model at the solid/solution interface: a theoretical analysis, J. Mol. Liq. 277 (2019) 646–648.

[21] Y. Ibrahim, V. Naddeo, F. Banat, S.W.J.S. Hasan, P. Technology, Preparation of Novel Polyvinylidene Fluoride (PVDF)-Tin(IV) Oxide (SnO2) Ion Exchange Mixed Matrix Membranes for the Removal of Heavy Metals from Aqueous Solutions, 2020, p. 250.

[22] A. Ja, A. Ro, A. Smrn, B. Ss, Electrochemical storage reactions of hydrogen in activated carbon from phenolic resin, Catal. Today 397–399 (2021) 155–164.

[23] D. Khandare, S. Mukherjee, 'A review of metal oxide nanomaterials for fluoride decontamination from water environment, Mater. Today Proc. 11 (2019) 46–55.

[24] M. Kobya, E. Demirbas, E. Senturk, M. Ince, Adsorption of heavy metal ions from aqueous solutions by activated carbon prepared from apricot stone, Bioresour. Technol. 96 (2005) 1518–1521.

[25] H. Li, X. Dong, E.B. da Silva, L.M. de Oliveira, Y. Chen, L.Q. Ma, Mechanisms of metal sorption by biochars: biochar characteristics and modifications, Chemosphere 178 (2017) 466–478.

[26] Y. Li, X. Chen, L. Liu, P. Liu, Z. Zhou, Y. Huhetaoli Wu, T. Lei, Characteristics and adsorption of Cr(VI) of biochar pyrolyzed from landfill leachate sludge, J. Anal. Appl. Pyrol. 162 (2022), 105449.

[27] N. Liu, Y. Zhang, C. Xu, P. Liu, J. Lv, Y. Liu, Q. Wang, Removal mechanisms of aqueous Cr(VI) using apple wood biochar: a spectroscopic study, J. Hazard Mater. 384 (2020) 121–371.

[28] W. Liu, J. Zhang, C. Zhang, L. Ren, Preparation and evaluation of activated carbon-based iron-containing adsorbents for enhanced Cr(VI) removal: mechanism study, Chem. Eng. J. 189–190 (2012) 295–302.

[29] X.-J. Liu, M.-F. Li, J.-F. Ma, J. Bian, F. Peng, Chitosan crosslinked composite based on corncob lignin biochar to adsorb methylene blue: kinetics, isotherm, and thermodynamics, Colloids Surf. A Physicochem. Eng. Asp. 642 (2022), 128621.

[30] R. Ma, X. Yan, X. Pu, X. Fu, L. Bai, Y. Du, M. Cheng, J. Qian, An exploratory study on the aqueous Cr(VI) removal by the sulfate reducing sludge-based biochar, Separ. Purif. Technol. 276 (2021).

[31] W. Mao, L. Zhang, Y. Zhang, Y. Wang, N. Wen, Y. Guan, Adsorption and photocatalysis removal of arsenite, arsenate, and hexavalent chromium in water by the carbonized composite of manganese-crosslinked sodium alginate, Chemosphere 292 (2022).

[32] T. Masinga, M. Moyo, V.E. Pakade, Removal of hexavalent chromium by polyethyleneimine impregnated activated carbon: intra-particle diffusion, kinetics and isotherms, J. Mater. Res. Technol. 18 (2022) 1333–1344.

[33] K.J. Min, J.H. Kim, K.Y. Park, Characteristics of heavy metal separation and determination of limiting current density in a pilot-scale electrodialysis process for plating wastewater treatment, Sci. Total Environ. 757 (2021), 143762.

[34] N. Mohamad Nor, L.C. Lau, K.T. Lee, A.R. Mohamed, Synthesis of activated carbon from lignocellulosic biomass and its applications in air pollution control—a review, J. Environ. Chem. Eng. 1 (2013) 658–666.

[35] Mohammad Boshir Ahmed, Md Abu Hasan Johir, John L. Zhou, Huu Hao Ngo, Long Duc Nghiem, Christopher Richardson, Mohammad Ali Moni, Macguire R. Bryant, Activated carbon preparation from biomass feedstock: clean production and carbon dioxide adsorption, J. Clean. Prod. 225 (2019) 405–413.

[36] V.-T. Nguyen, T.-B. Nguyen, C.-W. Chen, C.-M. Hung, T.-D.-H. Vo, J.-H. Chang, C.-D. Dong, Influence of pyrolysis temperature on polycyclic aromatic hydrocarbons production and tetracycline adsorption behavior of biochar derived from spent coffee ground, Bioresour. Technol. 284 (2019) 197–203.

[37] E.C. Nnadozie, P.A. Ajibade, Data for experimental and calculated values of the adsorption of Pb(II) and Cr(VI) on APTES functionalized magnetite biochar using Langmuir, Freundlich and Temkin equations, Data Brief 32 (2020), 106292.

[38] D. Ouyang, Y. Chen, J. Yan, L. Qian, L. Han, M. Chen, Activation mechanism of peroxymonosulfate by biochar for catalytic degradation of 1,4-dioxane: important role of biochar defect structures, Chem. Eng. J. 370 (2019) 614–624.

[39] S.J. Peighambardoust, R. Foroutan, S.H. Peighambardoust, H. Khatooni, B. Ramavandi, Decoration of Citrus limon wood carbon with Fe_3O_4 to enhanced Cd^{2+} removal: a reclaimable and magnetic nanocomposite, Chemosphere 282 (2021) 131, 088.

[40] A.A. Prakash, A. Rajasekar, R.K. Sarankumar, M.S. AlSalhi, S. Devanesan, M.J. Aljaafreh, M. Govarthanan, S.R.M. Sayed, Metagenomic analysis of microbial community and its role in bioelectrokinetic remediation of tannery contaminated soil, J. Hazard Mater. 412 (2021) 125–133.
[41] E.D. Revellame, D.L. Fortela, W. Sharp, R. Hernandez, M.E. Zappi, Adsorption kinetic modeling using pseudo-first order and pseudo-second order rate laws: a review, Clean. Eng. Technol. 1 (2020), 100032.
[42] A. Rf, A. Sjp, B. Aa, A. Aa, C. Sf, D. J. J. o Br, C.E. E, Adsorption Mercury, Cobalt, and Nickel with a Reclaimable and Magnetic Composite of hydroxyapatite/Fe_3O_4/polydopamine, 2021.
[43] A. Rv, B. Pkm, A. Ss, Comprehensive investigation of the mechanism for Cr(VI) removal from contaminated water using coconut husk as a biosorbent, J. Clean. Prod. 314 (2021) 117–128.
[44] B. Saha, C. Orvig, Biosorbents for hexavalent chromium elimination from industrial and municipal effluents, Coord. Chem. Rev. 254 (2010) 2959–2972.
[45] R. Saha, R. Nandi, B. Saha, Sources and toxicity of hexavalent chromium, J. Coord. Chem. 64 (2011).
[46] P. Samiyammal, A. Kokila, L.A. Pragasan, R. Rajagopal, R. Sathya, S. Ragupathy, M. Krishnakumar, V.R. Minnam Reddy, Adsorption of brilliant green dye onto activated carbon prepared from cashew nut shell by KOH activation: studies on equilibrium isotherm, Environ. Res. 212 (2022), 113497.
[47] A. Saravanan, P.S. Kumar, M. Govarthanan, C.S. George, S. Vaishnavi, B. Moulishwaran, S.P. Kumar, S. Jeevanantham, P.R. Yaashikaa, Adsorption characteristics of magnetic nanoparticles coated mixed fungal biomass for toxic Cr(VI) ions in aquatic environment, Chemosphere 267 (2021), 129226.
[48] J. Serafin, M. Ouzzine, C. Xing, H. El Ouahabi, A. Kamińska, J. Sreńscek-Nazzal, Activated carbons from the Amazonian biomass and iroba shells applied as a CO2 adsorbent and a cheap semiconductor material, J. CO2 Util. 62 (2022), 102071.
[49] R. Shan, Y. Shi, J. Gu, J. Bi, H. Yuan, B. Luo, Y. Chen, Aqueous Cr(VI) removal by biochar derived from waste mangosteen shells: role of pyrolysis and modification on its absorption process, J. Environ. Chem. Eng. 8 (2020).
[50] B. Shen, G. Li, F. Wang, Y. Wang, C. He, M. Zhang, S. Singh, Elemental mercury removal by the modified bio-char from medicinal residues, Chem. Eng. J. 272 (2015) 28–37.
[51] J. Shen, G. Huang, C. An, X. Xin, C. Huang, S. Rosendahl, Removal of Tetrabromobisphenol A by adsorption on pinecone-derived activated charcoals: synchrotron FTIR, kinetics and surface functionality analyses, Bioresour. Technol. 247 (2018) 812–820.
[52] M. Su, Y. Fang, B. Li, W. Yin, J. Gu, H. Liang, P. Li, J. Wu, Enhanced hexavalent chromium removal by activated carbon modified with micro-sized goethite using a facile impregnation method, Sci. Total Environ. 647 (2019) 47–56.
[53] L. Tan, Y. Zhang, W. Zhang, R. Zhao, Y. Ru, T. Liu, One-pot method to prepare lignin-based magnetic biosorbents for bioabsorption of heavy metal ions, Ind. Crop. Prod. 176 (2022).
[54] X. Tan, Y. Liu, G. Zeng, X. Wang, X. Hu, Y. Gu, Z. Yang, Application of biochar for the removal of pollutants from aqueous solutions, Chemosphere 125 (2015) 70–85.
[55] C.A. Uko, J.O. Tijani, S.A. Abdulkareem, S. Mustapha, T.C. Egbosiuba, E. Muzenda, Adsorptive properties of MgO/WO3 nanoadsorbent for selected heavy metals removal from indigenous dyeing wastewater, Process Saf. Environ. Protect. 162 (2022) 775–794.
[56] B. Wang, Y.S. Jiang, F.Y. Li, D.Y. Yang, Preparation of biochar by simultaneous carbonization, magnetization and activation for norfloxacin removal in water, Bioresour. Technol. 233 (2017) 159–165.
[57] D. Wang, J. Pan, D. Zhu, Z. Guo, C. Yang, X. Duan, Enhanced adsorption of NO onto activated carbon by gas pre-magnetization, Sci. Total Environ. 830 (2022), 154712.
[58] J. Wang, S. Chen, J.Y. Xu, L.C. Liu, J.C. Zhou, J.J. Cai, High-surface-area porous carbons produced by the mild KOH activation of a chitosan hydrochar and their CO_2 capture, N. Carbon Mater. 36 (2021) 1081–1090.
[59] Y. Wang, C. Peng, E. Padilla-Ortega, A. Robledo-Cabrera, A. López-Valdivieso, Cr(VI) adsorption on activated carbon: mechanisms, modeling and limitations in water treatment, J. Environ. Chem. Eng. 8 (2020), 104031.
[60] S. Xia, Z. Song, P. Jeyakumar, S.M. Shaheen, J. Rinklebe, Y.S. Ok, N. Bolan, H. Wang, A critical review on bioremediation technologies for Cr(VI)-contaminated soils and wastewater, Crit. Rev. Environ. Sci. Technol. 49 (2019) 1027–1078.
[61] X. Xu, H. Huang, Y. Zhang, Z. Xu, X. Cao, Biochar as both electron donor and electron shuttle for the reduction transformation of Cr(VI) during its sorption, Environ. Pollut. 244 (2019) 423–430.
[62] H. Yang, S. Ye, H. Wang, C. Zhou, T. Xiong, Y. Deng, Q. Fu, G. Zeng, Z. Zeng, X. Tan, Insight into disinfection byproduct formation potential of aged biochar and its effects during chlorination, J. Environ. Manag. 317 (2022) 115–437.
[63] J.-C. Yoo, C. Lee, J.-S. Lee, K. Baek, Simultaneous application of chemical oxidation and extraction processes is effective at remediating soil Co-contaminated with petroleum and heavy metals, J. Environ. Manag. 186 (2017) 314–319.
[64] N. Zaitseva, V. Zaitsev, A. Walcarius, Chromium(VI) removal via reduction-sorption on bi-functional silica adsorbents, J. Hazard Mater. 250 (2013) 454–461.
[65] Z.Q. Zhang, Z.F. Meng, Z.Y. p, The derivation of Freundlich kinetic equation and exploration on the physical meaning of its parameters, J. NW A F Univ.: Nat. Sci. Ed. 31 (2003) 202–204.
[66] M. Zhao, Z. Huang, S. Wang, L. Zhang, Ultrahigh efficient and selective adsorption of Au(III) from water by novel Chitosan-coated MoS2 biosorbents: performance and mechanisms, Chem. Eng. J. 401 (2020), 126006.
[67] Y.-F. Zhou, R.J. Haynes, Sorption of heavy metals by inorganic and organic components of solid wastes: significance to use of wastes as low-cost adsorbents and immobilizing agents, Crit. Rev. Environ. Sci. Technol. 40 (2010) 909–977.